scientific reports

Check for updates

OPEN

Removal of the nalidixic acid antibiotic from aqueous solutions using bovine serum albumin nanoparticles

Masoumeh Ghahremani[1], Hossein Danafar[2,4], Parastoo Afshari[1], Mehran Mohammadian Fazli[3] & Hamed Bahrami[1]✉

The presence of antibiotic pollutants in water and wastewater can cause significant risks to the environment in different aspects. Therefore, antibiotics need to be removed from water. This study investigates the adsorption of nalidixic acid (NA), a common antibiotic, using bovine serum albumin nanoparticles (BSA NPs). These NPs were synthesized *via* desolvation technique and characterized using SEM, DLS, FT-IR, and UV-Vis spectroscopy. The effects of adsorbent dosage (0.02–0.9 mg), initial NA concentration (30–80 mg L^{-1}) and contact time (0.5–24 h) on adsorption efficiency were considered. Adsorption isotherms and kinetics were determined experimentally. The Freundlich isotherm best described the adsorption equilibrium, while the pseudo-second-order kinetic model accurately represented the adsorption process. Thermodynamic parameters confirmed the spontaneous and exothermic nature of NA adsorption onto BSA NPs. Under optimal conditions, BSA NPs achieved a removal efficiency of 75% for NA with a maximum adsorption capacity of 240 mg g^{-1}. These results demonstrate the potential of BSA NPs as an effective adsorbent for removing NA from aqueous solutions.

Keywords Bovine serum albumin nanoparticles (BSA NPs), Adsorption, Nalidixic acid, Wastewater treatment

The contamination of water by organic pollutants, especially pharmaceutical contaminants, is a cause for concern worldwide[1]. Antibiotics, among the myriad of water contaminants, have garnered significant research attention due to their association with the emergence of antibiotic-resistant bacteria, commonly known as superbugs[2]. Since these drugs are not completely metabolized in the body of human and animal, 30–90% of the administered antibiotics are excreted in the urine and finally, feces to wastewater. Due to their continuous entry and stability in aquatic ecosystems, antibiotics can lead to the spread of antibiotic-resistant bacteria in the environment, even at very low concentrations[3,4]. As a result, the human body becomes resistant to antibiotics due to the constant ingestion of these drugs through drinking water and the resistance of pathogens. Recent studies have shown that conventional wastewater treatment processes are ineffective at completely removing pharmaceuticals, leading to their discharge into aquatic environments. Consequently, there is an urgent need to develop efficient, sustainable, and economically viable strategies for pharmaceutical removal from wastewater effluents[5,6].

Nalidixic acid (NA) is a synthetic antimicrobial agent classified as a quinolone. Structurally, it is derived from the 1,8-naphthyridine core. Historically, NA has been employed in the treatment of urinary tract infections caused by susceptible bacterial strains[7]. Several studies have reported its appearance in environmental waters, hospital effluents, and sewage treatment plants discharges. For example, the maximum concentrations of NA in hospital wastewater, wastewater from municipal sewage treatment plants, and environmental water were given as 0.45, 0.4, and 0.75 μg L^{-1}, respectively[8]. There are reports indicating the involvement of this drug in chronic toxicity and carcinogenicity, and its dangerousness for human health, therefore, much attention has been paid to remove this pollutant[9,10].

[1]Department of Chemistry, University of Zanjan, Zanjan 38791-45371, Iran. [2]Zanjan Pharmaceutical Nanootechnology Research Center, Zanjan University of Medical Sciences, Zanjan, Iran. [3]Department of Environmental Health Engineering, School of Public Health, Zanjan University of Medical Sciences, Zanjan, Iran. [4]Department of Medicinal Chemistry, School of Pharmacy, Zanjan University of Medical Sciences, Zanjan 45139-56184, Iran. ✉email: hbahrami@znu.ac.ir

Several techniques have been investigated for removal of antibiotics from water, each with its own limitations. Membrane filtration[11], while effective in removing antibiotics, is hindered by fouling, energy consumption, and membrane degradation. Advanced oxidation processes (AOPs)[12] provide efficient antibiotic degradation but suffer from high energy demands, by-product formation, and chemical reagent requirements. Biological treatment[13] is limited by the emergence of antibiotic resistance, prolonged treatment times, and environmental sensitivity. Photocatalysis[14] offers a sustainable approach but faces challenges in efficiency, catalyst deactivation, and practical application. Among the aforementioned techniques, surface adsorption has advantages over other methods in terms of efficiency, cost, operation simplicity, and removable pollutant concentration range. Commonly utilized adsorbents include activated carbon[15,16], clay minerals[17], zeolites[18], biochar[19], metal-organic frameworks (MOFs)[20], and carbon-based nanomaterials[21]. While these materials exhibit varying degrees of adsorption capacity and selectivity, challenges such as regeneration, potential for secondary pollution, and limited selectivity persist. Optimization of adsorbent properties and process conditions is crucial to mitigate these limitations and achieve effective contaminant removal. The development of novel adsorbents for wastewater treatment is an ongoing area of research. For example, recyclable O-g-C3N4/GO/N-CNT membranes[22] and cranberry kernels bio-waste[23] have emerged as promising biosorbents. Additionally, metal-organic frameworks (MOFs) with tailored pore structures[24], covalent organic frameworks (COFs) exhibiting high surface areas[25], and Two-dimensional metal borides (MBenes) with a large amount of oxygen-containing functional groups on their surface[26], have shown potential for efficient contaminant removal.

Previous studies have reported the efficacy of various methods for the removal of NA from aqueous solutions. These include ozonation[27], activated carbon derived from keratin waste[28], UV and UV/H_2O_2 processes[29], three-dimensional graphene cathodes[30], and adsorption onto anionic and neutral exchange polymers[31]. Additionally, the adsorptive capacity of graphene oxide (GO) for NA has been investigated[32].

Among nanoparticles (NPs), albumin-based NPs have attracted the attention of researchers owing to their special characteristics, including non-toxicity, solubility in water, and biodegradability, rendering them promising building block for nano-adsorbents[33]. BSA NPs have been reported as suitable drug carriers in the body[34]. BSA presents a promising candidate for nano-absorbent development. Its abundance as a cattle industry byproduct offers potential for low-cost production and scalability. The biocompatible nature of BSA mitigates environmental concerns. Protein-based materials often exhibit high stability under specific conditions, a property that could enhance nano-absorbent reliability. While BSA is a well-characterized protein with diverse applications, its efficacy as a nano-absorbent for water contaminant removal remains largely unexplored. Potential advantages include low-cost production, biocompatibility, and potentially high adsorption capacity due to BSA's complex molecular structure. However, critical challenges such as limited data on contaminant removal efficiency, and comparison to established technologies must be addressed before practical application. To the best of our knowledge, the adsorptive removal of dissolved NA from water using BSA NPs has not been previously reported.

The aim of the study is to investigate the potential of BSA NPs for the adsorptive removal of NA from aqueous solutions. BSA NPs were synthesized *via* the desolvation method. To elucidate the adsorption behavior, the effects of initial NA concentration, adsorbent dosage, contact time, and temperature were examined. Additionally, adsorption isotherm and kinetic models were applied to describe the adsorption process. To the best of our knowledge, this study constitutes the first reported application of BSA NPs as an adsorbent for the removal of NA. Our findings indicate that BSA NPs present a novel, efficient, readily accessible, environmentally friendly, and promising adsorbent for the elimination of antibiotics from wastewater.

Experimental section

Reagents and equipment

NA was purchased from Merck (Germany). BSA, N-(3-dimethylaminopropyl)-N-ethylcarbodiimide hydrochloride (EDC), and phosphate buffer (PBS) were obtained from Sigma-Aldrich (St. Louis, USA). Sodium hydroxide (NaOH) and hydrochloric acid (HCl) from Merck (Germany) were acquired for pH adjustment. All working solutions were prepared using distilled water. The pH of solutions was measured using Metrohm/827 pH meter. An incubation shaker (Heidolph Titramax) facilitated sample mixing, and an Eppendorf 5418 centrifuge separated the adsorbent from the samples. The initial and final concentrations of NA solutions were determined by an ion mobility spectrometer (model IMS 300) from TOF Tech Pars CO. (Isfahan, Iran).

Synthesis of BSA NPs

BSA NPs have been prepared the use of the desolvation approach as explained in previous studies[35,36]. Initially, 16 ml of ethanol was added gradually to the 8 ml BSA solution (62.5 mg ml^{-1}) at a rate of 2 ml min^{-1}. The solution was continuously stirred (1250 rpm with a 1 cm magnet, at room temperature) until the appearance of turbidity, indicating NP formation. To enhance particle stability, EDC (10 mg in 200 µl water) was introduced for crosslinking purposes. Stirring was extended for three hours to complete the crosslinking process.

Sample characterization

BSA NPs were investigated by Scanning Electron Microscope (SEM) imaging, dynamic light scattering (DLS), FT-IR, and UV–Vis techniques. SEM analyses were conducted with KYKY-EM8000F (KYKY Technology CO. Ltd, China). Mean particle size, hydrodynamic size distribution, and zeta potential of developed hybrid system were determined by using DLS on a nano/zetasizer (Malvern Instruments, Worcestershire, UK, ZEN 3600 model Nano ZS). FT-IR diagnostics were used to determine the chemical composition of the BSA NPs. This analysis was performed with a Bruker Tensor 27 FTIR instrument in the range of 400 to 4000 square centimeters. The absorption spectrum of the synthesized NPs was measured by a spectrometer (model GENESYS 10 S; UV-vis) 600 to 200 nm wavelength (Thermo Fisher Scientific, Madison, Wisconsin).

Adsorption experiments

The initial NA solution (1000 mg l^{-1}) was prepared by dissolving 10 mg NA in 10 ml distilled water. The desired concentrations for the experiments were prepared by diluting the stock solution. The adsorption process was carried out in an aqueous solution at a temperature of 25 °C and a neutral pH of 7.2. The experiments were carried out using 2 ml microtubes. A certain amount of BSA adsorbent was added to each microtube containing the test solution, and the total volume of each microtube was adjusted to 2 ml. After the optimal conditions were set, the samples were shaken in the incubator at a speed of 80 rpm for 24 h. Then the samples were centrifuged at 13,000 rpm for 10 min to separate the NPs. To investigate the effect of adsorbent dosage, different amounts of BSA NPs (0.02–0.9 mg) were mixed with 2 ml of 80 mg l^{-1} NA solution for 24 h. The concentration of NA remaining in the solution after treatment (equilibrium concentration, C_e) was measured by ion mobility spectrometry (IMS). The initial concentration of NA in the test solution (C_0) was also determined using IMS. The calibration curve for NA was prepared by plotting the average signal obtained from three repetitions of IMS spectrum recording for each solution with a certain concentration.

The percentage removal (R%) and equilibrium adsorption capacity (q_e) were calculated using Eqs. (1) and (2):

$$\mathrm{R}\% = \frac{(C_0 \_ C_e)}{C_0} \times 100 \tag{1}$$

$$q_e = \frac{(C_0 \_ C_e)V}{m} \tag{2}$$

where C_0 and C_e (mg l^{-1}) are the initial and equilibrium concentrations of NA, respectively. m (g) is the weight of the BSA NPs, and V (L) is the total volume of the solution.

The ability of BSA NPs for removal of NA was examined by addition of 0.5 mg of BSA to 2 mL NA solution with concentration range of 5–80 mg l^{-1}, and shaking for 24 h. The percentage of removed NA was calculated using Eq. (1). The obtained data for this factor were used to investigate the adsorption mechanism of NA onto BSA NPs. Langmuir, Freundlich, Temkin, and Dubinin–Raduschevich isotherm models were examined for this purpose.

To determine the rate of NA removal and the maximum adsorption equilibrium time and to understand the kinetics of the adsorption process, 2 ml solutions were prepared with an initial concentration of 80 mg l^{-1}. Then 0.5 mg of the adsorbent was added to the samples. The samples were stirred at different time intervals (30, 1, 2, 3, 4, 5, and 24 h). After the desired time, the samples were immediately removed and centrifuged at 13,000 rpm for 10 min. Finally, the concentration of NA remaining in the aqueous phase was measured by IMS. The amount of drug absorbed at time t, which is called absorption capacity at instant t (q_t), was determined using Eq. (3). The collected data were used to determine the rate-controlling step of the adsorption process by applying pseudo-first-order (PFO), pseudo-second-order (PSO), and intraparticle diffusion (IPD) kinetic models.

$$q_t = \frac{(C_0 \_ C_t)V}{m} \tag{3}$$

where C_t (mg l^{-1}) is the remaining concentration of NA at time t.

To investigate the influence of temperature on the adsorption process, experiments were conducted by adding 0.5 mg of BSA to 2 ml of an 80 mg l^{-1} NA solution at temperatures ranging from 25 to 55 °C. Thermodynamic parameters were subsequently determined using the van't Hoff equation.

Results and discussion

Characterization of the NPs

Particle size and morphology

BSA NPs were prepared according to our previously reported method[35]. The formation and characterization of BSA NPs and BSA NPs loaded with NA were confirmed through DLS analysis and SEM imaging. The DLS data provided insights into the size distribution and surface charge of the NPs, while the SEM images offered a detailed view of their morphology.

Panels (a) and (b) in Fig. 1 present the size distribution by intensity for both the BSA NPs and BSA-NA NPs. The BSA NPs exhibited a relatively uniform size distribution, with an average size of approximately 280.1 nm as indicated by the sharp peak in Panel (a). After loading with NA, Panel (b) shows an increase in particle size, where the average size shifted to 333.8 nm, confirming successful drug adsorption.

The zeta potential measurements, shown in Panels (c) and (d), provided information about the surface charge of the NPs, which is crucial for understanding their stability and interaction with biological environments. The BSA NPs had a zeta potential of – 6.47 mV, indicating a slightly negative surface charge, which helps in maintaining a stable dispersion in solution (Panel c). Upon drug loading, the zeta potential of the NPs shifted to – 30.7 mV, as shown in Panel (d), suggesting changes in surface properties due to the interaction with NA. The observed shift in zeta potential of the NPs upon the addition of a drug solution is attributable to the anionic state of NA at pH 7.2.

Panels (e) and (f) show SEM images that provide a visual assessment of the morphology of the NPs. The BSA NPs, depicted in Panel (e), displayed a globular shape and homogeneous spherical morphology with a smooth surface, which is characteristic of well-formed NPs. After drug loading, the BSA-NA NPs in Panel (f) exhibited a rougher surface with a slight degree of aggregation, suggesting successful drug adsorption on the NP surface.

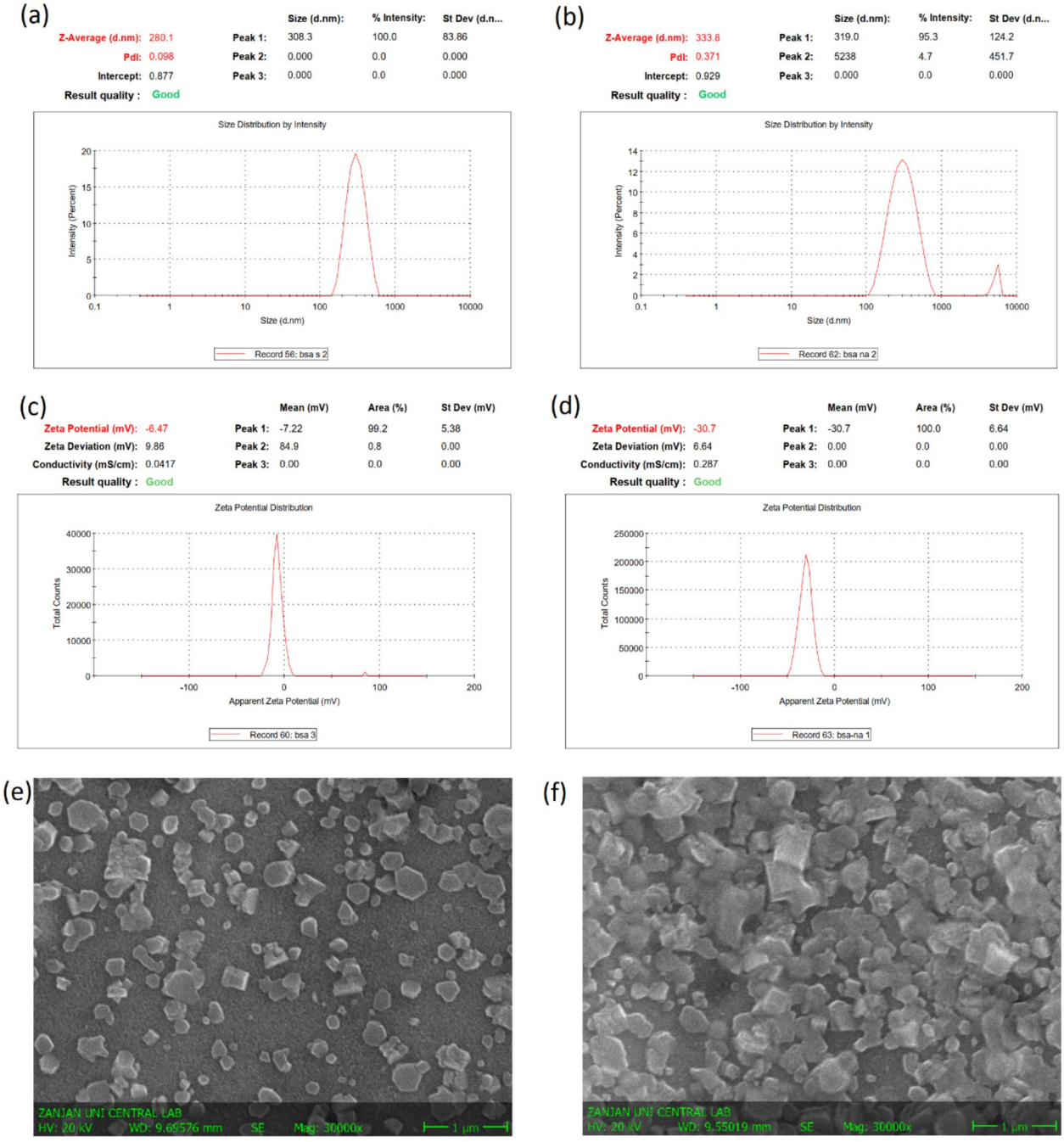

Fig. 1. Size distribution by intensity of (a) BSA, (b) BSA-NA, ζ-potential of (c) BSA, (d) BSA-NA, and SEM of (e) BSA, (f) BSA-NA.

The SEM analysis further supports the findings from the DLS measurements, where the observed morphological changes align with the increased particle size and altered surface charge. These combined results demonstrate the effective loading of NA into BSA NPs, confirming their potential use in drug delivery applications.

FT-IR analysis

FT-IR method was used to confirm the synthesis of BSA and NA adsorption to BSA. FT-IR spectra of BSA NPs fore-and-after NA adsorption are presented in (Fig. 2).

In the spectrum of pure NA (Fig. 2a), there are various absorption peaks in the areas of 3500 cm^{-1} corresponding to acidic (O–H), 3000 cm^{-1} corresponding to (C–H) stretching, 1633 cm^{-1} corresponding

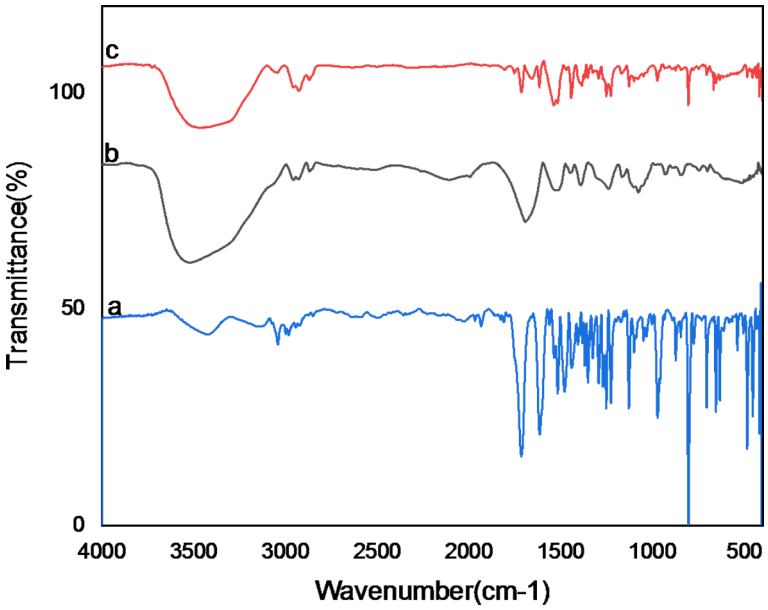

Fig. 2. FT-IR spectra of (a) pure NA, (b) pure BSA, and (C) BSA-NA.

to (C=C), 1700 cm^{-1} corresponding to (C=O) carbonyl group, 1110 cm^{-1} corresponds to) C–O) ether and 800 cm^{-1} corresponds to benzene ring[37]. In the FT-IR spectrum of pure BSA (Fig. 2b), different absorption peaks in the regions of 1644 cm^{-1} (amide I) and 1525 cm^{-1} (amide II) are shown[38]. In the BSA-NA spectrum (Fig. 2C), the peaks corresponding to the amide I and II groups in BSA are slightly shifted. This displacement indicates the interaction between the amide groups of BSA and NA. Also, the amide peak intensity has increased in the spectrum (Fig. 2C). In addition, a new peak appears in the spectrum of BSA-NA at 1660, which corresponds to the carbonyl group in NA.

UV-Vis spectrophotometric analysis

To confirm the adsorption of NA by BSA, the UV-Vis absorption spectra of NA, BSA and BSA-NA were compared in (Fig. 3). The UV-Vis spectrum of BSA shows an absorption peak at 281 nm[38] (Fig. 3a). As can be seen in (Fig. 3b), two peaks are observed in the spectrum of NA in the range of 258–335 nm[39]. As depicted in Fig. 3c, the characteristic peaks corresponding to both BSA and NA are also present in the BSA-NA spectrum. In the BSA-NA absorption spectrum compared to that of BSA, a change in shape and the shift in the peaks is observed[40] that indicates the absorption of NA on BSA.

Effect of adsorbent dosage

The effect of adsorbent dosage, ranging from 0.02 to 0.9 mg, was investigated at pH 7.2 and an initial NA concentration of 80 mg l^{-1}.

As shown in Fig. 4, increasing the adsorbent dosage from 0.02 to 0.5 mg resulted in increased NA removal. Beyond a dosage of 0.5 mg, the removal percentage plateaued, indicating minimal sensitivity to further adsorbent additions. This plateau suggests that the adsorbent's active sites became saturated after approximately 0.5 mg, with subsequent increases in dosage having a negligible effect on removal efficiency.

Initial NA concentration and adsorption isotherms

The initial concentration range of NA was chosen from 30 to 80 mg l^{-1} to investigate the removal efficiency of NPs. For this purpose, the adsorbent dose and volume of NA solution were selected as 0.5 mg and 2 ml, respectively.

As demonstrated in Fig. 5, the removal efficiency obtained for the lowest concentration was 68% and for the highest concentration was 75%. This 7% increase in adsorption efficiency could be due to the increased number of NA molecules available to interact with BSA NPs. The optimal initial concentration of NA was chosen to be 80 ppm.

To understand the relationship between adsorbed species and their equilibrium concentrations, different isothermal models such as Langmuir, Freundlich, Temkin, and Dubinin–Raduschevich were evaluated. The parameters of the four isothermal models were fitted using the equilibrium data (Table 1).

Langmuir isotherm A certain number of sites for adsorption exist on the surface. Each site binds to an adsorbed molecule (adsorption is a monolayer). The interaction energy is the same for all adsorption sites[41,42]. The linear equation of the Langmuir isotherm is shown as Eq. (4).

$$\frac{q_e}{C_e} = bq_{max} - bq_e \tag{4}$$

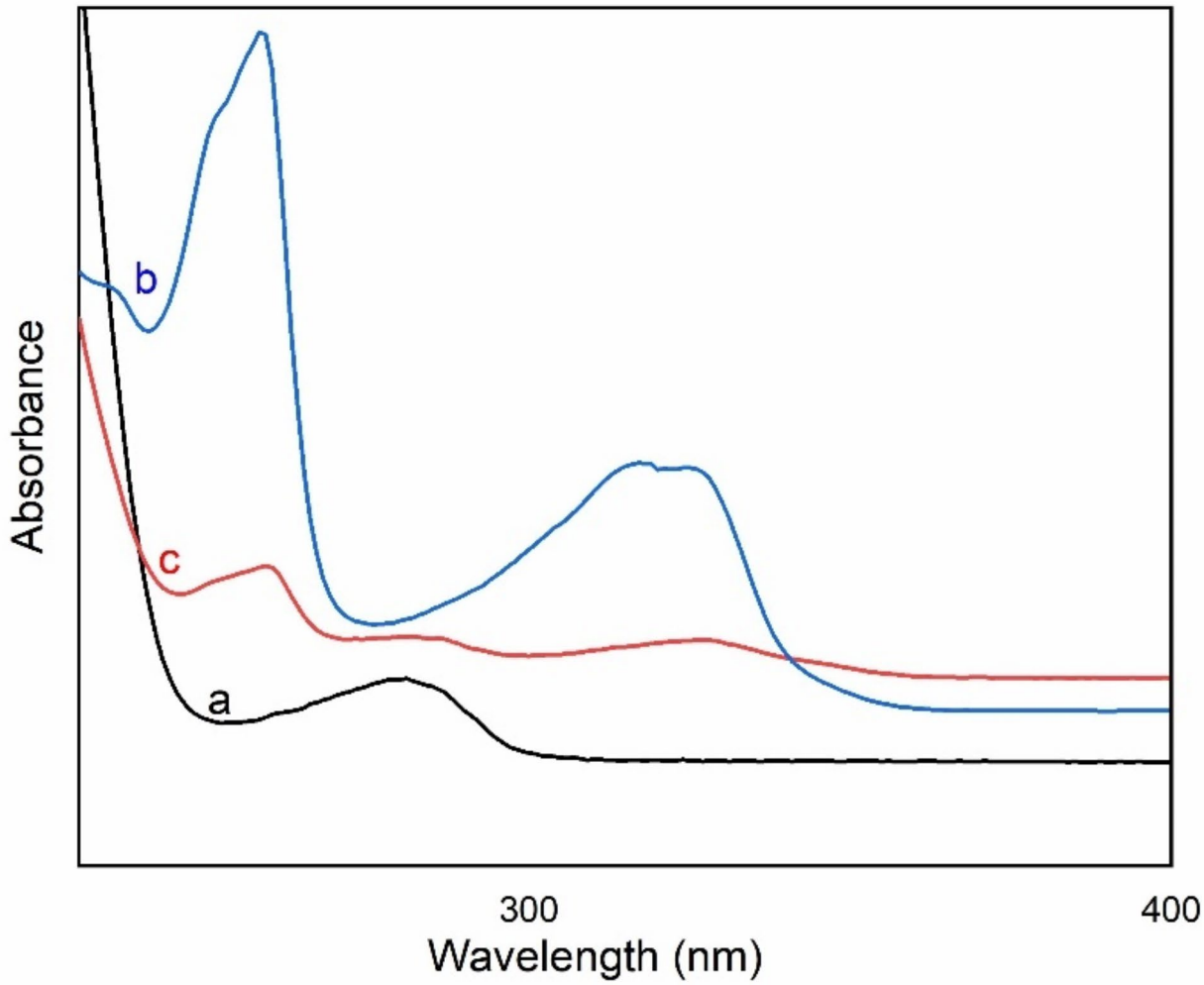

Fig. 3. UV-Vis absorption spectra of (a) pure BSA, (b) pure NA, and (C) BSA-NA.

b and q_{max} are the Langmuir adsorption constant and the maximum adsorption capacity, respectively. The values of b and q_{max} can be obtained by plotting the curve of q_e/C_e against q_e (Fig. 6a).

Freundlich isotherm It is primarily relevant to heterogeneous surfaces and multilayer adsorption. Multilayer surface adsorption results in an uneven distribution of energy[43]. The linear equation of the Freundlich isotherm is as follows.

$$logq_e = logK_f + {}^{1}\!/_{n}\, logC_e \tag{5}$$

log q_e is plotted against log C_e to determine the absorption capacity (K_f) and the absorption intensity (n) (Fig. 6b).

Temkin isotherm This model acknowledges that the binding energy can vary across the surface. It specifically considers that the heat of adsorption (a measure of the binding energy) decreases linearly as the surface coverage increases. This means the initial adsorption sites are the most favorable energetically, and subsequent adsorption becomes progressively less favorable[44]. The Temkin isotherm model presents a unique approach compared to the Langmuir and Freundlich models by considering the impact of surface coverage on the free energy of sorption. This model is suitable for situations involving various adsorption sites and changes in enthalpy as the surface coverage increases. Temkin isotherm is introduced by Eq. (6).

$$q_e = B_T lnK_T + B_T lnC_e \tag{6}$$

The plot of q_e versus ln C_e has a slope of B_T (J mol^{-1}) that is the Temkin constant. The equilibrium binding constant (K_T) is obtained from intercept magnitude of the plot (Fig. 6c).

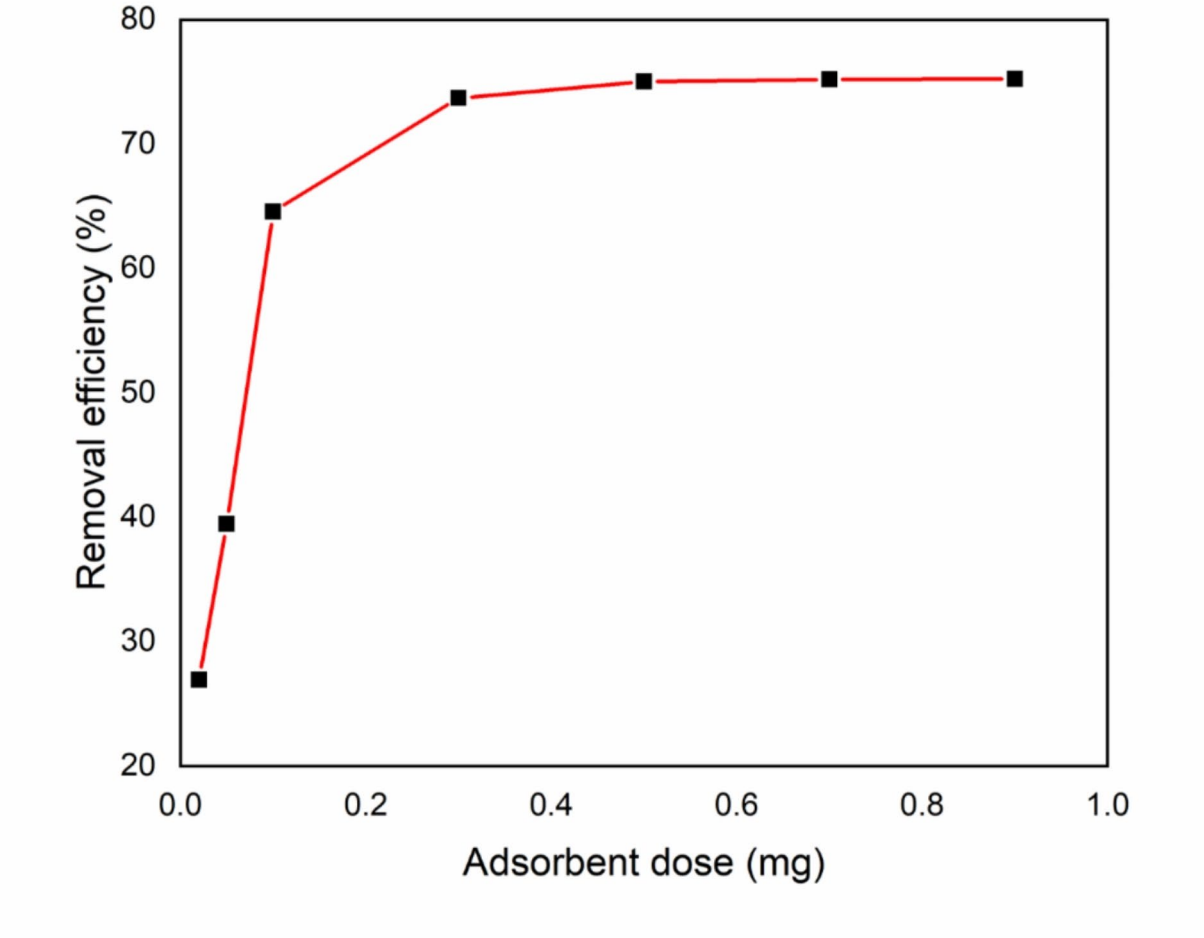

Fig. 4. Effect of adsorbent dosage on NA adsorption onto BSA NPs. (Conditions: initial NA concentration = 80; dosage of adsorbent = variable; pH = 7.2; contact time = 24 h; solution temperature = 25 °C).

Dubinin-Raduschevich isotherm The Dubinin–Radushkevich (D–R) isotherm model does not assume a uniform or constant adsorption potential across the surface. The D–R isotherm is described by the following Eq. (7)

$$lnq_e = lnq_m - K_{D-R}\epsilon^2 \tag{7}$$

where, K_{D-R} ($mol^2\ J^{-2}$) is a constant related to the adsorption energy, and ϵ^2 is the Polanyi potential, defined by Eq. (8):

$$\epsilon = RTln\left(1 + \frac{1}{C_e}\right) \tag{8}$$

Plotting ln q_e against ε^2 enables the determination of the parameters K_{D-R} and q_m. The mean adsorption energy (E) in kJ mol^{-1}, which indicates the energy required to transfer one mole of adsorbate from an infinite distance to the adsorbent surface, can be calculated as follows (9):

$$E = \frac{1}{\sqrt{2K}} \tag{9}$$

When the calculated value of E is less than 8 kJ mol^{-1}, the adsorption process is typically classified as physical adsorption. If the value of E falls between 8 and 16 kJ mol^{-1}, the adsorption process can be explained by a chemical adsorption mechanism[45] (Fig. 6d).

The results of these four isotherms are presented in Table 1.

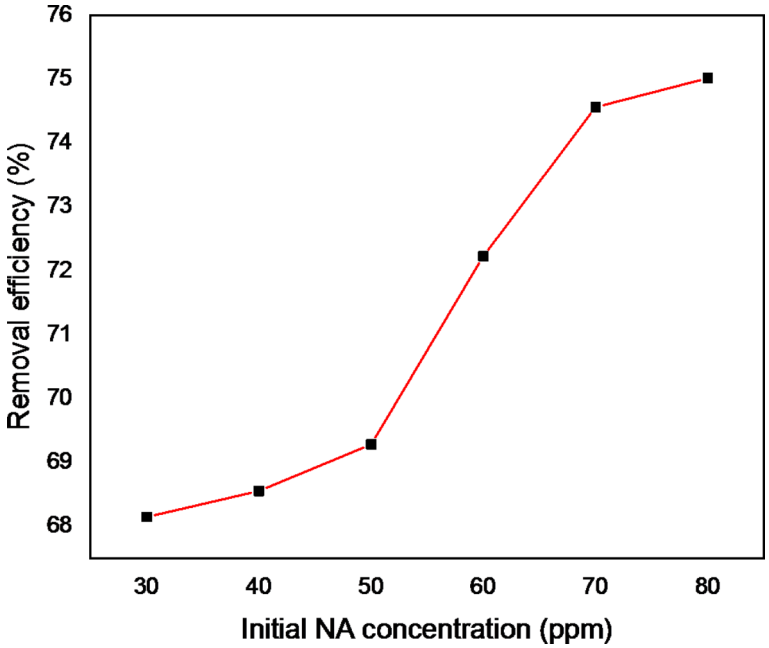

Fig. 5. The effect of initial NA Concentration on the value of NA adsorbed on BSA NPs. (Conditions: initial NA concentration = variable; dosage of adsorbent = 0.5 mg; pH = 7.2; contact time = 24 h; solution temperature = 25 °C)

isotherm model	parameters	Value
Langmuir	q_{max} (mg g^{-1})	246.05
$q_e/C_e = bq_{max} - bq_e$	b (l mg^{-1})	0.0249
	R^2	0.94
Freundlich	n	0.67
$\log q_e = \log K_f + 1/n logC_e$	K_f (mg l^{-1})	2.64
	R^2	0.96
Temkin	B_T	213.52
$q_e = B_T lnK_T + B_T lnC_e$	k_T (l g^{-1})	0.141
	R^2	0.89
D–R	q_{max}(mg g^{-1})	283.95
$lnq_e = lnq_m - K_{D-R}\epsilon^2$	K_{D-R} (mol^2 kJ^{-2})	22.169
	E (kJ mol^{-1})	0.150
	R^2	0.87

Table 1. Isotherm models' parameters for adsorption of NA onto BSA NPs.

Langmuir isotherm suggests specific and restricted binding sites on the BSA NPs for the NA molecules. The obtained parameters, including q_{max} of 246.05 mg g^{-1} and the b of 0.0249 l mg^{-1}, are evidences that confirm the favorable absorption and that there are well-defined binding sites for NA on the BSA NPs. Freundlich isotherm implies multilayer adsorption, where NA molecules can accumulate on the surface of the BSA NPs. The values of the intensity of adsorption (n) of 0.67 and the adsorption capacity (K_f) of 2.64 mg l^{-1} suggest that the adsorption process is heterogeneous and that the interaction between NA and BSA NPs is not uniform. The R^2 value (0.89) for the Temkin model is lower than those for the Langmuir and Freundlich models, suggesting that it is not as good a fit for the data. In the Dubinin-Radushkevich isotherm, the adsorption energy was determined to be 0.17 kJ mol^{-1}. Since adsorption energies below 8 kJ mol^{-1} are characteristic of physical adsorption, it can be concluded that the adsorption of NA by BSA is physical in nature. In conclusion, the Freundlich isotherm was found to be the most suitable model for describing the adsorption of NA onto BSA NPs.

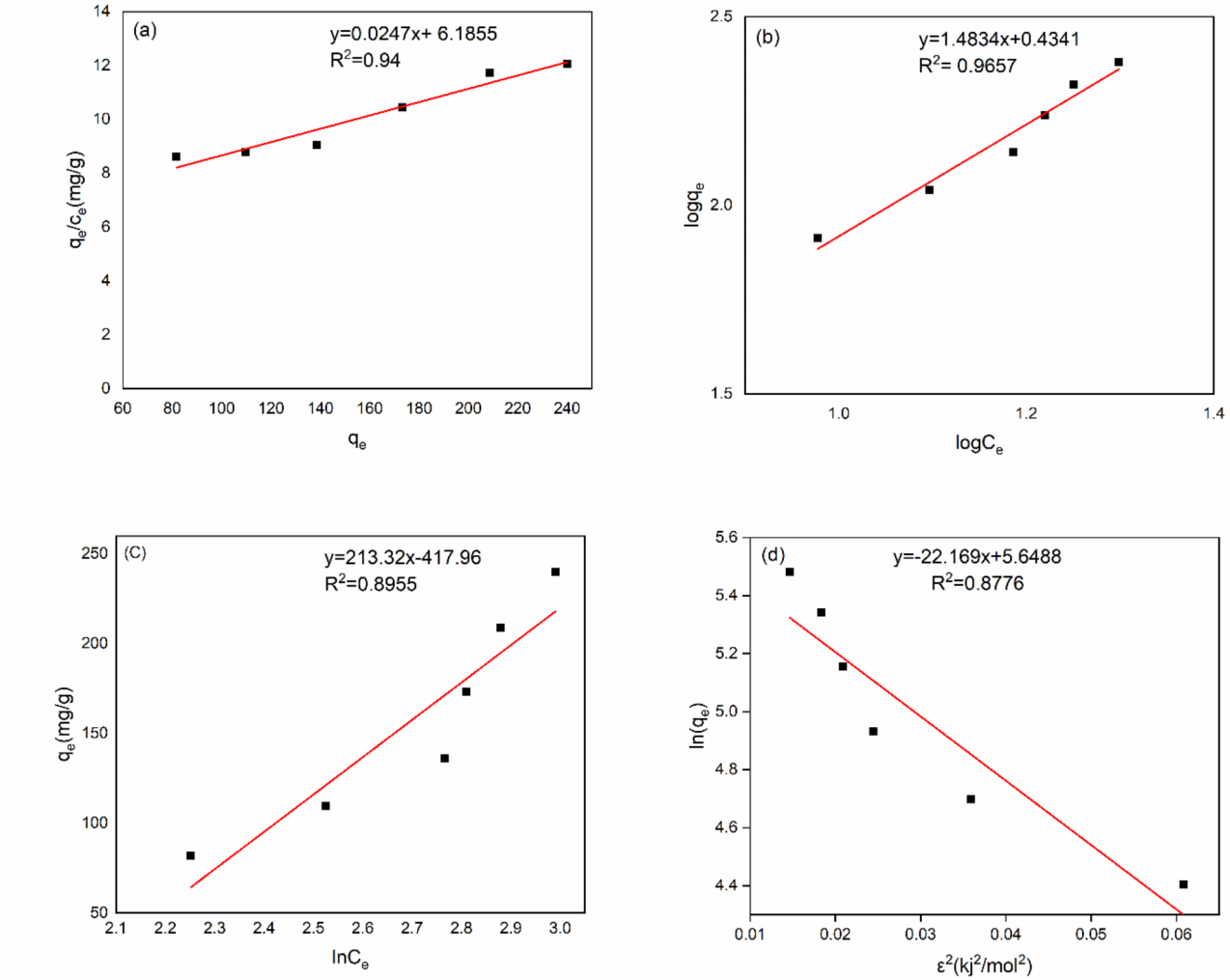

Fig. 6. plots of isotherm models for NA adsorption on BSA NPs (a) Langmuir, (b) Freundlich, (c) Temkin, and (d) Dubinin-Radushkevich isotherm.

Kinetic study

The kinetics of adsorption offers valuable insights into understanding both the rate and the mechanism of adsorption reactions. Contact time is a critical factor for achieving a successful adsorption process. Dependence of NA removal by BSA NPs on interaction time was investigated under different time intervals (0.5–24 h).

As can be seen in Fig. 7, increasing the contact time has a direct effect on the R% as well as q_e. The absorption rate of NA was initially fast until it reached equilibrium after about 5 h. At the beginning of the absorption process, a significant number of active sites were available, but as the process continued, these sites were gradually occupied by drug molecules. The determined R% for the concentration of 80 mg l^{-1} NA was 75%, reaching an equilibrium after about 5 h in which most of the NA is removed. After reaching equilibrium, extending the contact time no longer has much effect due to the reduction of adsorbent active sites. The highest value for q_e was observed as 240 mg g^{-1} for the solution with the highest initial concentration of NA. According to the results, 5 h was chosen as the optimal interaction time for 80 mg l^{-1} concentration.

To investigate the kinetics of NA absorption by BSA NPs, PFO, PSO and, IPD kinetic models were used[46]. The parameters of these three models are presented in Table 2.

The PFO rate equation commonly referred to as the Lagergren equation, is typically used to depict the adsorption of solutes onto adsorbents[47]. The equation is as follows:

$$\ln(q_e - q_t) = \ln q_e - k_{1t} \quad (10)$$

where k_1 (min^{-1}) is the PFO rate constant. In Fig. 8a, the PFO kinetic plots display the relationship between $\ln(q_e - q_t)$ and t.

The PSO linear kinetic equation is as follows[48]:

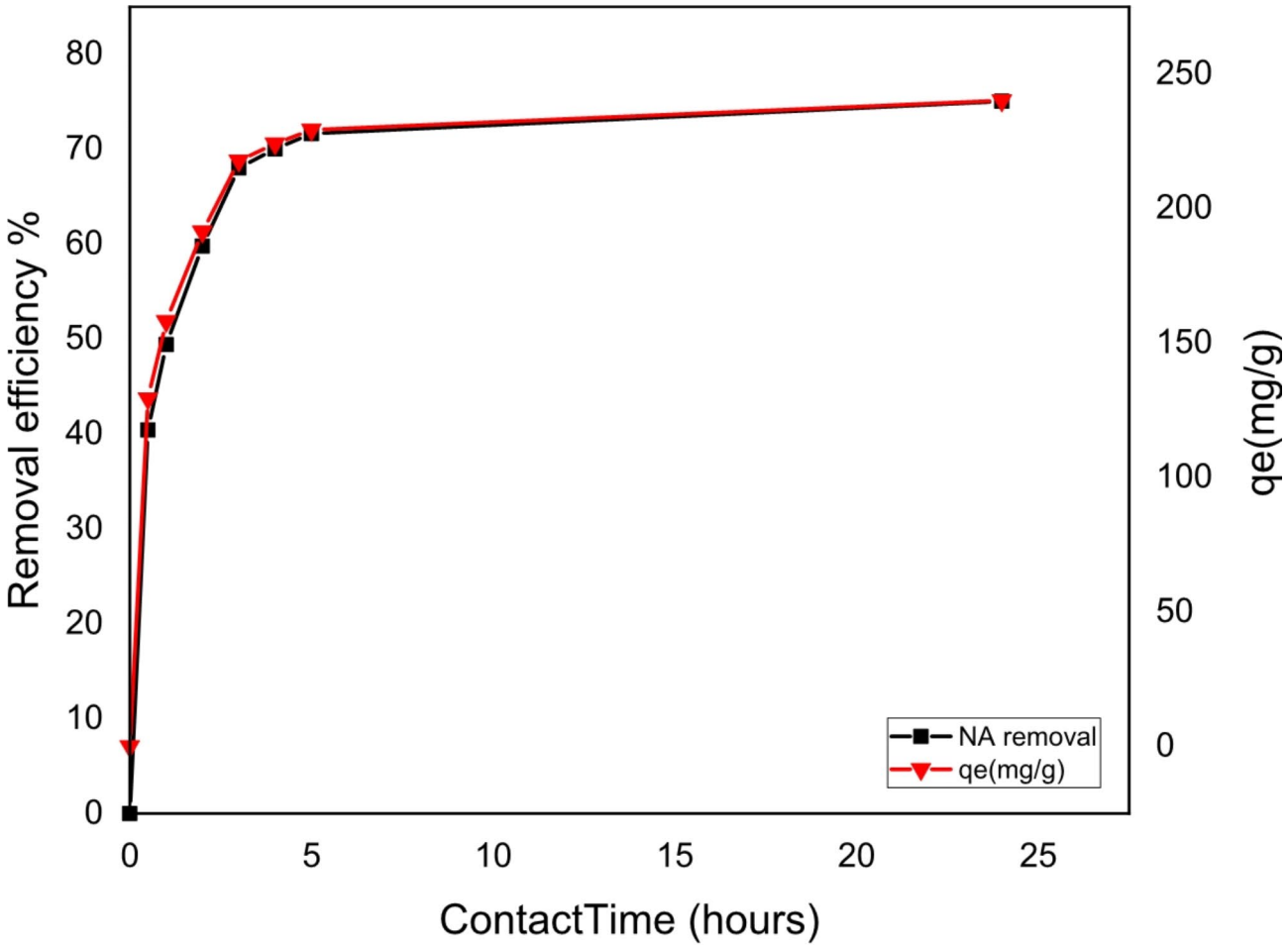

Fig. 7. The effect of interaction time on the value of NA adsorbed on BSA NPs. (Conditions: initial NA concentration 80 ppm; dosage of adsorbent = 0.5 mg; pH = 7.2; contact time = variable (0.5–24 h), solution temperature = 25 °C).

Kinetic model	Parameters	Value
PFO	k_1 (min^{-1})	−0.10592
$\ln(q_e\text{-}q_t) = \ln q_e - k_1 t$	q_e (exp) (mg g^{-1})	136.15
	q_e (cal)	240.05
	R^2	0.9846
PSO	k_2 (mg g^{-1} min^{-1})	0.00691
$\frac{t}{q_t} = \frac{1}{k_2 q_e^2} + \frac{t}{q_e}$	q_e (exp) (mg g^{-1})	256.41
	q_e (cal)	240.05
	R^2	0.99
IPD	K (mg g^{-1} $min^{-1/2}$)	98.684
$q_t = k_{int}\sqrt{t} + C$	C	36.068
	R^2	0.90

Table 2. Kinetic parameters for the PFO, PSO, and IPD Kinetic models.

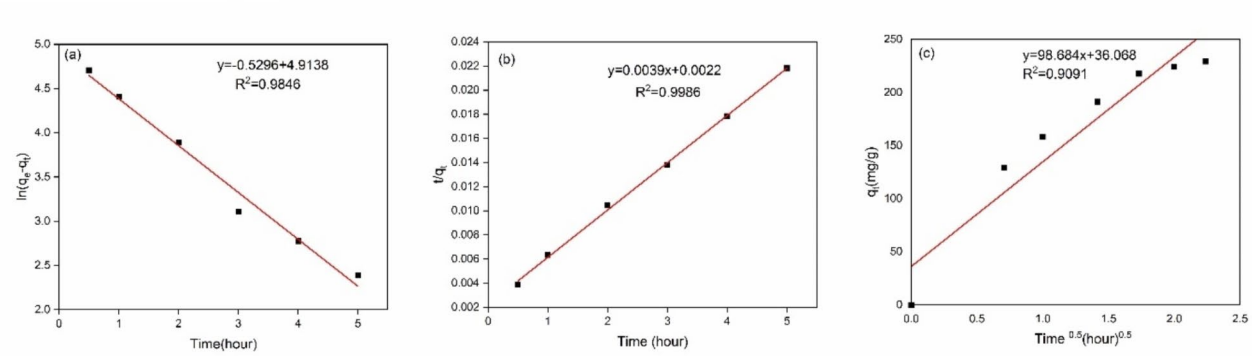

Fig. 8. (a) PFO, (b) PSO, and (C) IPD kinetic curves for interaction of NA with BSA NPs.

Adsorbent	Max adsorption capacity (mg g^{-1})	Best-fitted isotherm model	Best-fitted Kinetic Model	References
Layered double hydroxide-graphene oxide-chitosan (LDH-GO-CS NC))	277.79	Freundlich	PSO	9
Montmorillonite and kaolinite	–	Freundlich	PSO	50
Nanometric magnetite	137.2(μmol g^{-1})	Freundlich	PSO	51
Carbon nanotubes (CNT)	186	Freundlich		52
Carbon nanofibers (CNF)	67	Freundlich		52
high surface area graphite (HSAG)	179	Freundlich		52
multi-wall non-functionalized carbon nanotubes (MWCNT)	111	Freundlich	–	53
CNT functionalized with COOH groups (MWCNT-COOH)	79	Freundlich	-	53
CNT functionalized with NH_2 groups (MWCNT-NH_2)	98	Freundlich	-	53
BSA NPs	240	Freundlich	PSO	This study

Table 3. Adsorption performances of different adsorbents for NA removal.

$$\frac{t}{q_t} = \frac{1}{k_2 q_e^2} + \frac{t}{q_e} \tag{11}$$

where k_2 is the PSO rate constant (mg g^{-1} min^{-1}). This constant is obtained from intercept magnitude of the t/q_t against t plot (Fig. 8b).

To describe the IPD model, one must consider the steps involved in the uptake of adsorbate by the adsorbent including: bulk diffusion, film diffusion, intra-particle diffusion in the solid phase, and adsorption on the surface. Considering the intra-particle diffusion in the solid phase as the rate-controlling step, the mathematical equation describing the adsorption process is given by the Weber and Morris[49] equation:

$$q_t = k_{int}\sqrt{t} + C \tag{12}$$

where k_{int} is the intra-particle diffusion equation constant (mg g^{-1} $min^{-0.5}$) and C is a constant. The plot of q_t versus $t^{0.5}$ for the intraparticle diffusion model shown in Fig. 8c. This model predicts a linear relationship between the amount adsorbed (q_t) and the square root of time ($\sqrt{t}$) when diffusion influences the adsorption rate. If intra-particle diffusion is the sole rate-determining step, the line should pass through the origin (C = 0).

The parameters of each model, along with their coefficients of determination (R^2), are shown in Table 2. According to the obtained results, the R^2 value for the PSO model is higher than that of the PFO, and PID models. Additionally, the experimental absorption capacity (q_e exp) of the PSO model is closer to the calculated absorption capacity (q_e cal). In addition, the non-zero value of the constant "C" in the IPD model indicates that factors other than IPD influence the adsorption process. Consequently, this model is not reliable for examining NA onto the BSA NPs adsorption kinetics. Therefore, the adsorption of NA onto the BSA NPs is described by the PSO kinetic mode.

Comparison of adsorption behavior based on literature data

The removal efficiency of NA onto BSA NPs adsorbent was assessed with regard to its adsorption capacity of other sorbents, the comparison summarized in Table 3. Our literature review has shown that the adsorption of NA on different adsorbents often follows the Freundlich isotherm and the PSO kinetic model. As shown, q_{max} of BSA NPs (240 mg g^{-1} for adsorbent dose 0.5 mg l^{-1}, and at 25°) has shown an acceptable value, compared

to other absorbents. The comparison results point to this fact that the BSA NPs show very good prospect of adsorbing NA.

Adsorption thermodynamics

Absorption experiments were conducted within a temperature range of 298–328 K to determine thermodynamic parameters. The Gibbs free energy (ΔG°), Enthalpy (ΔH°) and entropy ($\Delta S°$) changes for the adsorption process were calculated using the following equations[54].

$$\Delta G^{\circ} = -RT\ln\ (K_l) \tag{13}$$

$$lnK_l = \frac{\Delta S^{\circ}}{R} - \frac{\Delta H^{\circ}}{R} \tag{14}$$

In these equations, T represents the absolute temperature (K), R is the gas constant (J mol^{-1} K^{-1}), and K_l is the thermodynamic equilibrium constant, equal to the ratio of the adsorbed amount (q_e) to the equilibrium concentration (C_e). Figure 9 shows the linear plot of ln K_l versus 1/T. The obtained values for thermodynamic parameters are shown in Table 4.

The negative ΔG° values indicate that the adsorption process of NA onto BSA is spontaneous. The decreasing magnitude of ΔG° with increasing temperature (from −6.15 to − 5.70 kJ mol^{-1}) suggests a decrease in spontaneity, potentially due to reduced adsorption or increased desorption. The negative ΔH° value (– 10.36 kJ mol^{-1}) confirms the exothermic nature of the adsorption process. Additionally, the negative ΔS° value (– 14.17 J $mol^{-1}K^{-1}$) implies a decrease in system disorder upon adsorption, likely attributed to restricted molecular motion of NA on the BSA surface. Therefore, the adsorption of NA onto BSA NPs is spontaneous and exothermic.

Mechanism of adsorption

The proposed adsorption mechanism of NA onto BSA NPs involves a complex interplay of intermolecular forces. Hydrogen bonding between nalidixic acid's carbonyl group and BSA's amide groups is a key interaction

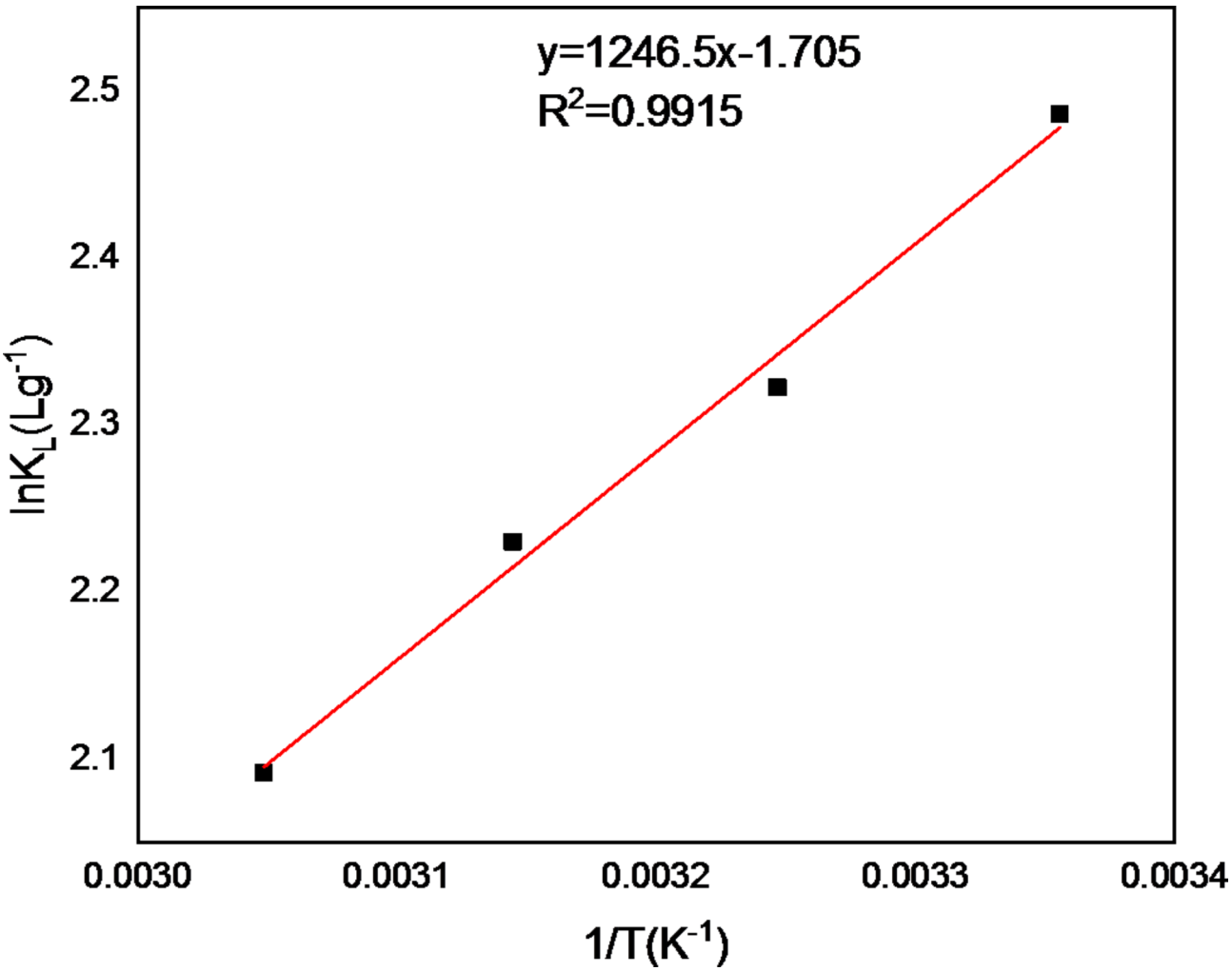

Fig. 9. Thermodynamics plot for obtaining the ΔH° and ΔS° of NA adsorption by BSA NPs.

Temperature (K)	ΔG° (kJ mol^{-1})	ΔH° (kJ mol^{-1})	ΔS° (J mol^{-1} K^{-1})
298	− 6.15	− 10.36	− 14.17
308	− 5.94		
318	− 5.89		
328	− 5.70		

Table 4. Thermodynamic parameters for NA adsorption onto BSA.

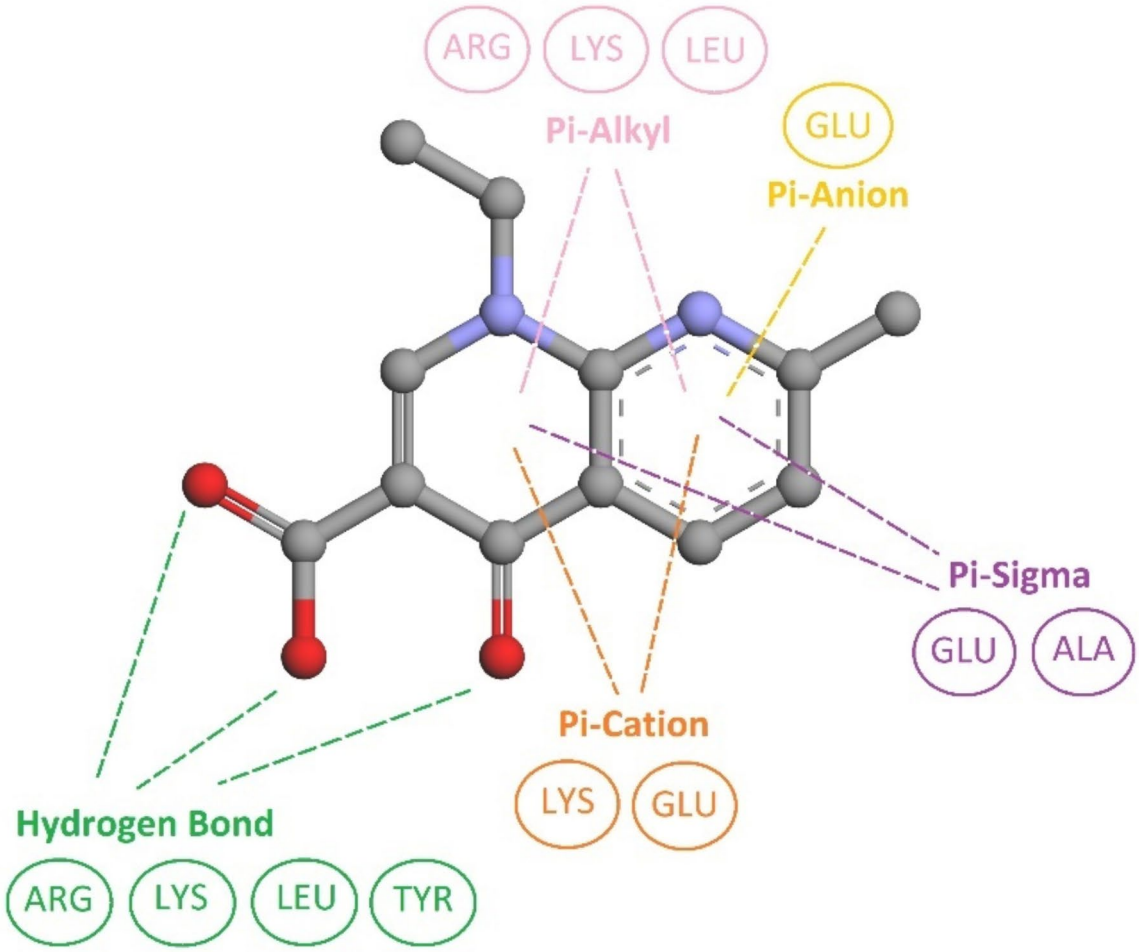

Fig. 10. Schematic diagram of the interaction between NA and residues in the surface of BSA NPs.

supported by FT-IR data. Hydrophobic interactions between nonpolar regions of both molecules likely contribute significantly to the adsorption process (Fig. 10). While electrostatic repulsion exists due to the negative charges, local charge variations could result in attractive electrostatic interactions. Additionally, π-π interactions between the aromatic structures of NA and potential aromatic amino acids in BSA might play a role. Conformational changes in BSA upon adsorption could further influence the adsorption process. The relative contributions of these interactions require further investigation through experimental and computational methods.

Conclusions

This study investigated the efficacy of BSA NPs for removing NA from aqueous solutions. The BSA NPs were successfully synthesized and characterized using various techniques. The adsorption process was significantly influenced by factors such as adsorbent dosage, initial NA concentration, and contact time. The Freundlich isotherm model best described the adsorption equilibrium, suggesting a multilayer adsorption mechanism. Kinetic studies revealed that the PSO model effectively represented the adsorption kinetics. Thermodynamic

analysis demonstrated that the adsorption of NA onto BSA NPs was spontaneous and exothermic. Notably, the BSA NPs achieved a maximum adsorption capacity of 240 mg g^{-1} for NA under optimal conditions.

These findings demonstrate the potential of BSA NPs as a promising adsorbent for removing NA from water. To realize this potential, future research should focus on enhancing the material's reusability, stability, and efficiency in real wastewater conditions. Additionally, exploring the removal of other contaminants is essential. Overcoming challenges related to material engineering and economic viability will be crucial for the successful application of this technology.

Data availability

The datasets used during the current study available from the corresponding author on reasonable request.

Received: 23 June 2024; Accepted: 24 September 2024
Published online: 15 October 2024

References

1. Mukhopadhyay, A., Duttagupta, S. & Mukherjee, A. Emerging organic contaminants in global community drinking water sources and supply: a review of occurrence, processes and remediation. *J. Environ. Chem. Eng.* **10**, 107560. https://doi.org/10.1016/j.jece.2022.107560 (2022).
2. Koch, N., Islam, N. F., Sonowal, S., Prasad, R. & Sarma, H. Environmental antibiotics and resistance genes as emerging contaminants: methods of detection and bioremediation. *Curr. Res. Microb. Sci.* **2**, 100027. https://doi.org/10.1016/j.crmicr.2021.100027 (2021).
3. Flach, K. A. et al. Antibiotic resistant bacteria and genes (ARB and ARG) in water and sewage treatment units: a review. *Environ. Nanatechnol. Monit. Manage.* **21**, 100941. https://doi.org/10.1016/j.enmm.2024.100941 (2024).
4. Wang, J. et al. Risk control of antibiotics, antibiotic resistance genes (ARGs) and antibiotic resistant bacteria (ARB) during sewage sludge treatment and disposal: a review. *Sci. Total Environ.* **877**, 162772. https://doi.org/10.1016/j.scitotenv.2023.162772 (2023).
5. Gorovits, R., Sobol, I., Akama, K., Chefetz, B. & Czosnek, H. Pharmaceuticals in treated wastewater induce a stress response in tomato plants. *Sci. Rep.* **10**, 1856. https://doi.org/10.1038/s41598-020-58776-z (2020).
6. Radovic, S., Pap, S., Niemi, L. & Prodanović, J. Turk Sekulic, M. A review on sustainable technologies for pharmaceutical elimination in wastewaters—a ubiquitous problem of modern society. *J. Mol. Liq.* **383**, 122121. https://doi.org/10.1016/j.molliq.2023.122121 (2023).
7. Dube, P. S., Legoabe, L. J. & Beteck, R. M. Quinolone: a versatile therapeutic compound class. *Mol. Divers.* **27**, 1501–1526. https://doi.org/10.1007/s11030-022-10581-8 (2023).
8. Watkinson, A., Murby, E., Kolpin, D. W. & Costanzo, S. The occurrence of antibiotics in an urban watershed: from wastewater to drinking water. *Sci. Total Environ.* **407**, 2711–2723 (2009).
9. Radmehr, S., Hosseini Sabzevari, M., Ghaedi, M., Ahmadi Azqhandi, M. H. & Marahel, F. Adsorption of nalidixic acid antibiotic using a renewable adsorbent based on graphene oxide from simulated wastewater. *J. Environ. Chem. Eng.* **9**, 105975. https://doi.org/10.1016/j.jece.2021.105975 (2021).
10. Sharma, M. K. et al. A snapshot on the development of quinolones and fluoroquinolones-an origin of nalidixic acid. *Herb. Med. J.* **9**, 56. https://doi.org/10.22087/hmj.v9i2.887 (2024).
11. Liu, H., Zhang, H., Dong, X., Wu, C. & Lichtfouse, E. Removal of antibiotics from black water by a membrane filtration-visible light photocatalytic system. *J. Water Process. Eng.* **53**, 103605. https://doi.org/10.1016/j.jwpe.2023.103605 (2023).
12. Wang, X., Jing, J., Zhou, M. & Dewil, R. Recent advances in H2O2-based advanced oxidation processes for removal of antibiotics from wastewater. *Chin. Chem. Lett.* **34**, 107621. https://doi.org/10.1016/j.cclet.2022.06.044 (2023).
13. Lu, Z., Liu, G., Xie, H., Zhai, Y. & Li, X. Advances and solutions in biological treatment for antibiotic wastewater with resistance genes: a review. *J. Environ. Manage.* **368**, 122115. https://doi.org/10.1016/j.jenvman.2024.122115 (2024).
14. Nguyen, T. D. et al. Multicomponent photocatalysts for synergic removal of antibiotics in aqueous media: a review. *Environ. Chem. Lett.* **21**, 935–980. https://doi.org/10.1007/s10311-022-01533-7 (2023).
15. Bednárek, J. et al. Revelation of high-adsorption-performance activated carbon for removal of fluoroquinolone antibiotics from water. *Biomass Convers. Biorefinery* **14**, 2585–2599. https://doi.org/10.1007/s13399-022-02577-z (2024).
16. Hashemzadeh, F., Ariannezhad, M. & Derakhshandeh, S. H. Sustainable removal of tetracycline and Paracetamol from water using magnetic activated carbon derived from pine fruit waste. *Sci. Rep.* **14**, 16346. https://doi.org/10.1038/s41598-024-65656-3 (2024).
17. Ciğeroğlu, Z. et al. Clay-based nanomaterials and their adsorptive removal efficiency for dyes and antibiotics: a review. *Mater. Today Sustain.* **26**, 100735. https://doi.org/10.1016/j.mtsust.2024.100735 (2024).
18. Al-Salihi, S., Fidalgo, M. M. & Xing, Y. Fast removal of tetracycline from aqueous solution by aluminosilicate zeolite nanoparticles with high adsorption capacity. *ACS ES&T Water* **3**, 838–847. https://doi.org/10.1021/acsestwater.2c00600 (2023).
19. Jia, Y. et al. Biochar-based strategies for antibiotics removal: mechanisms, factors, and application. *ACS ES&T Eng.* **4**, 1256–1274. https://doi.org/10.1021/acsestengg.3c00605 (2024).
20. Negro, C. et al. Multivariate)-metal–organic framework for highly efficient antibiotic capture from aquatic environmental matrices. *ACS Appl. Mater. Interfaces*. **15**, 3069–3076. https://doi.org/10.1021/acsami.2c20458 (2023).
21. Singh, R. et al. Processing of Carbon-based nanomaterials for the removal of pollutants from water/wastewater application. *Water* **15**, 3003 (2023).
22. Hayat, A. et al. Advances/Scope and prospects of g-C3N4 derived fascinating photocatalyst as a leading route towards solar energy adaption. *J. Clean. Prod.* **438**, 140568. https://doi.org/10.1016/j.jclepro.2024.140568 (2024).
23. Şenol, Z. M., Keskin, Z. S., Saraç, K. & Şimşek, S. Bioremoval of fast green FCF dye from aqueous solution using cranberry kernel (*Cornus mas* L.) as a lignocellulosic biowaste: equilibrium, kinetics, and mechanism. *Int. J. Environ. Anal. Chem.* **2023**, 1–18. https://doi.org/10.1080/03067319.2023.2201446 (2023).
24. Yue, J. et al. Cu–Co bimetallic organic framework as effective adsorbents for enhanced adsorptive removal of tetracycline antibiotics. *Sci. Rep.* **14**, 17607. https://doi.org/10.1038/s41598-024-67986-8 (2024).
25. Hayat, A. et al. Developing new-generation covalent organic frameworks as sustainable catalysts: synthesis, properties, types and solar energy production. *Mater. Sci. Eng. R: Rep.* **157**, 100771. https://doi.org/10.1016/j.mser.2024.100771 (2024).
26. Hayat, A. et al. Novel 2D MBenes-synthesis, structure, properties with excellent performance in energy conversion and storage: a review. *Mater. Sci. Eng. R: Rep.* **159**, 100796. https://doi.org/10.1016/j.mser.2024.100796 (2024).
27. Pollice, A. et al. Removal of nalidixic acid and its degradation products by an integrated MBR-ozonation system. *J. Hazard. Mater.* **203**, 46–52 (2012).
28. Wang, J., Liu, H. & Zhang, J. Antibiotic nalidixic acid removal by activated carbon prepared from keratin wastes. *Adv. Mater. Res.* **1004**, 895–899 (2014).
29. Kim, I., Yamashita, N. & Tanaka, H. Performance of UV and UV/H2O2 processes for the removal of pharmaceuticals detected in secondary effluent of a sewage treatment plant in Japan. *J. Hazard. Mater.* **166**, 1134–1140 (2009).

30. Zarei, M., Nahand, F. B., Khataee, A. & Hasanzadeh, A. Removal of nalidixic acid from aqueous solutions using a cathode containing three-dimensional graphene. *J. Water Process. Eng.* **32**, 100978 (2019).
31. Robberson, K., Waghe, A., Sabatini, D. & Butler, E. Adsorption of the quinolone antibiotic nalidixic acid onto anion-exchange and neutral polymers. *Chemosphere* **63**, 934–941 (2006).
32. Radmehr, S., Sabzevari, M. H., Ghaedi, M., Azqhandi, M. H. A. & Marahel, F. Adsorption of nalidixic acid antibiotic using a renewable adsorbent based on Graphene oxide from simulated wastewater. *J. Environ. Chem. Eng.* **9**, 105975 (2021).
33. Kim, H. & Lim, S. I. Adsorption of antibiotics on serum albumin nanoparticle. *Clean. Technol.* **27**, 55–60 (2021).
34. Yu, Z., Yu, M., Zhang, Z., Hong, G. & Xiong Q. Bovine serum albumin nanoparticles as controlled release carrier for local drug delivery to the inner ear. *Nanoscale Res Lett.* **9**(1), 343. https://doi.org/10.1186/1556-276X-9-343 (2014). PMID: 25114637; PMCID:PMC4106659.
35. Nosrati, H. et al. Bovine serum albumin: an efficient biomacromolecule nanocarrier for improving the therapeutic efficacy of chrysin. *J. Mol. Liq.* **271**, 639–646 (2018).
36. Jahanban-Esfahlan, A., Dastmalchi, S. & Davaran, S. A simple improved desolvation method for the rapid preparation of albumin nanoparticles. *Int. J. Biol. Macromol.* **91**, 703–709 (2016).
37. Nabipour, H., Sadr, M. H. & Thomas, N. Synthesis, controlled release and antibacterial studies of nalidixic acid–zinc hydroxide nitrate nanocomposites. *New J. Chem.* **40**, 238–244 (2016).
38. Nosrati, H., Danafar, H., Rezaeejam, H. & Gholipour, N. Rahimi-Nasrabadi, M. evaluation radioprotective effect of curcumin conjugated albumin nanoparticles. *Bioorg. Chem.* **100**, 103891 (2020).
39. Carnamucio, F., Aiello, D., Foti, C., Napoli, A. & Giuffrè, O. Aqueous chemistry of nalidixic acid and its complexes with biological relevant cations: a combination of potentiometric, UV spectrophotometric, MS and MS/MS study. *J. Inorg. Biochem.* **249**, 112366. https://doi.org/10.1016/j.jinorgbio.2023.112366 (2023).
40. Monti, S., Manet, I., Manoli, F., Capobianco, M. L. & Marconi, G. Gaining an insight into the photoreactivity of a drug in a protein environment: a case study on nalidixic acid and serum albumin. *J. Phys. Chem. B.* **112**, 5742–5754. https://doi.org/10.1021/jp711261n (2008).
41. Langmuir, I. The constitution and fundamental properties of solids and liquids. Part I. Solids. *J. Am. Chem. Soc.* **38**, 2221–2295 (1916).
42. Hao, Y. M., Man, C. & Hu, Z. B. Effective removal of Cu (II) ions from aqueous solution by amino-functionalized magnetic nanoparticles. *J. Hazard. Mater.* **184**, 392–399 (2010).
43. Gupta, V. K., Rastogi, A. & Nayak, A. Biosorption of nickel onto treated alga (*Oedogonium hatei*): application of isotherm and kinetic models. *J. Colloid Interface Sci.* **342**, 533–539 (2010).
44. Singh, R. & Bhateria, R. Experimental and modeling process optimization of lead adsorption on magnetite nanoparticles via isothermal, kinetics, and thermodynamic studies. *ACS Omega* **5**, 10826–10837 (2020).
45. Şenol, Z. M. & Arslanoğlu, H. Influential biosorption of lead ions from aqueous solution using sand leek (*Allium scorodoprasum* L.) biomass: kinetic and isotherm study. *Biomass Convers. Biorefinery*. https://doi.org/10.1007/s13399-024-05539-9 (2024).
46. Şenol, Z. M., Keskin, Z. S., Dinçer, E. & Ayed, A. B. Influential lead uptake using dried and inactivated-fungal biomass obtained from *Panaeolus papilionaceus*: biological activity, equilibrium, and mechanism. *Biomass Convers. Biorefinery*. https://doi.org/10.1007/s13399-024-05584-4 (2024).
47. Xu, P. et al. Synthesis of iron oxide nanoparticles and their application in *Phanerochaete chrysosporium* immobilization for pb (II) removal. *Colloids Surf. A* **419**, 147–155 (2013).
48. Ho, Y. S., Wase, D. J. & Forster, C. Kinetic studies of competitive heavy metal adsorption by sphagnum Moss peat. *Environ. Technol.* **17**, 71–77 (1996).
49. Weber Walter, J. & Morris, J. C. Kinetics of adsorption on carbon from solution. *J. Sanit. Eng. Div.* **89**, 31–59. https://doi.org/10.1061/JSEDAI.0000430 (1963).
50. Wu, Q., Li, Z. & Hong, H. Adsorption of the quinolone antibiotic nalidixic acid onto montmorillonite and kaolinite. *Appl. Clay Sci.* **74**, 66–73. https://doi.org/10.1016/j.clay.2012.09.026 (2013).
51. Usman, M. et al. Sorption of nalidixic acid onto micrometric and nanometric magnetites: experimental study and modeling. *Appl. Surf. Sci.* **299**, 136–145. https://doi.org/10.1016/j.apsusc.2014.01.197 (2014).
52. Patiño, Y., Díaz, E. & Ordóñez, S. Performance of different carbonaceous materials for emerging pollutants adsorption. *Chemosphere* **119**, S124–S130. https://doi.org/10.1016/j.chemosphere.2014.05.025 (2015).
53. Patiño, Y. et al. Adsorption of emerging pollutants on functionalized multiwall carbon nanotubes. *Chemosphere* **136**, 174–180. https://doi.org/10.1016/j.chemosphere.2015.04.089 (2015).
54. Şenol, Z. M., Ertap, H., Fernine, Y. & El Messaoudi, N. Adsorptive removal of synthetic dye from its aqueous solution by using chitosan-bentonite composite: DFT and experimental studies. *Polym. Bull.* https://doi.org/10.1007/s00289-024-05323-9 (2024).

Acknowledgements

We gratefully acknowledge the financial support from the Zanjan University of Medical Sciences and the University of Zanjan.

Author contributions

Masumeh Ghahremani: methodology, wrote the main manuscript, Hossein Danafar: Supervision, analysis of dates, Parastoo Afshari: methodology Mehran Mohammadian Fazli: revised the manuscript Hamed Bahrami: Supervision, analysis of dates.

Competing interests

The authors declare no competing interests.

Additional information

Correspondence and requests for materials should be addressed to H.B.

Reprints and permissions information is available at www.nature.com/reprints.

Publisher's note Springer Nature remains neutral with regard to jurisdictional claims in published maps and institutional affiliations.